M.M. Sarafraz, M. Jafarian, M. Arjomandi, G.J. Nathan
Potential of molten lead oxide for liquid chemical looping gasification (LCLG): a thermochemical analysis
International Journal of Hydrogen Energy, 2018; 43(9):4195-4210

Final publication at http://dx.doi.org/10.1016/j.ijhydene.2018.01.035

Potential of Molten Lead Oxide for Liquid Chemical Looping Gasification (LCLG): A Thermochemical Analysis

M. M. Sarafraz *, M. Jafarian, M. Arjomandi, G. J. Nathan

Centre for Energy Technology, School of Mechanical Engineering, University of Adelaide, SA 5005, Australia.

[*corresponding author]

Email: mohammadmohsen.sarafraz@adelaide.edu.au

Tel: +61416311335

Abstract

Molten lead oxide is revealed to have favourable thermodynamic performance for gasification in a new process employing chemical looping of a molten liquid metal oxide. In this process, the feedstock is partially oxidized with molten lead oxide in the fuel reactor, while the reduced molten lead is oxidized in the air reactor. As with other chemical looping processes, this avoids direct contact between air and fuel, which prevents the undesirable dilution of the gaseous product with nitrogen. The Gibbs minimization method was employed together with thermo-chemical equilibrium analysis to assess the feasibility of the gasification process using graphite as a surrogate for more realistic, but complex carbonaceous fuels, together with steam and/or carbon dioxide as the gasifying agent. It was found that both the reduction and oxidation reactions of molten lead oxide with carbonaceous fuel are spontaneous. Likewise, the ratio of H_2: CO can be as high as 2.5, while the carbon conversion can reach 94% based on the thermochemical analysis. An energetic performance analysis was also employed for the case of a supercritical steam turbine cycle to extract work from the hot gaseous co-products. On this basis, the first law efficiency of the power cycle was estimated to be up to 33.8%, while the

syngas co-product stream for applications such as Fischer-Trospsch synthesis has a chemical exergy efficiency of 41%.

Keywords: Liquid chemical looping gasification, molten lead, nitrogen dilution, power block, syngas production.

1. Introduction

Previous assessments of Chemical Looping Combustion (CLC) and Chemical Looping Gasification (CLG), an emerging processes under development (to produce energy and syngas, respectively) via reduction and oxidation of an oxygen carrier, have mostly been limited to materials in the solid state [1-3]. The driver for CLG is the potential to avoid direct contact between air and feedstock, whilst also providing the required heat for the gasification reactions, while the use of solid particles offers potential to develop novel materials with desirable properties. The process is performed in two interconnected reactors. The oxygen carrier is reduced in the reduction reactor and then transferred to the oxidation reactor, where it is oxidized with air [4, 5]. The potential advantages of CLG include the possibility of producing high-quality syngas (i.e. a high ratio of H_2 to CO) and to avoid nitrogen dilution without the need for expensive oxygen plant [5, 6]. However, its main disadvantages particularly for the case in which solid materials are used is high-temperature operation for the oxygen carrier and the challenge of cycling oxygen carriers for many cycles. The overall objective of the present paper is to assess the thermodynamic potential of a novel alternative configuration of CLG in which a liquid metal oxide (here lead oxide II) is employed to deliver net advantage over previously proposed cycles.

High-temperature operation of CLC and CLG systems with solid particles as the oxygen carrier causes morphological changes to the particles, such as sintering and agglomeration, which reduces their life [7, 8]. This challenge is particularly significant in the gasification reactor

because the oxygen-starved atmosphere generates unreacted carbon, which readily deposits onto the particles [9]. These carbon deposits then react with air in the oxidation reactor to generate wasted heat and carbon dioxide, significantly reducing the effectiveness of the oxygen transport and the efficiency of the process [5]. For example, the gasification of biomass using CLG reported by Acharya et al. [10] only achieved 40% regeneration of the CaO solid particles at a calcination temperature of 800°C. A low regeneration efficiency of 50% was also reported by Li et al. [11], with similar values reported elsewhere [5, 12-16]. It is also desirable to identify alternative approaches for chemical looping gasification that might bypass them altogether.

The use of a liquid metal oxide as the oxygen carrier for CLG offers potential to avoid the aforementioned technical challenges associated with the use of solid OC particles, but although brings alternative challenges such as the risk of solidification and the challenge of containment. However, before beginning to assess these other challenges and potential solutions, it is first necessary to assess the thermodynamic potential of the LCLG concept to identify whether the magnitude of the potential benefit is sufficient to justify the additional investment that would be needed to overcome the challenges. Hence, the objective of the present investigation is to meet this need.

Molten metals are well known to be effective for gasifying carbonaceous feedstock from previous works with high temperature metal-containing slags in blast furnaces [17, 18]. Molten slag is a by-product of the refining of metals such as iron and comprises a mixture of metal oxides such as SiO_2, Al_2O_3, CaO, FeO and MgO [19]. Molten slag typically leaves a blast furnace at temperatures of up to 1650 °C, so that it carries sufficient sensible heat resource to contribute to gasification. In the commercial application of this process, a carbonaceous fuel is partially oxidized, typically in the presence of a gasifying agent such as steam and/or CO_2, by injecting it into the high temperature molten slag. However, no systematic investigation is

available of the gasification of solid feedstock with pure liquid metal oxides or of their thermodynamic potential for chemical looping gasification.

The potential to harness the properties of molten iron/iron oxide to reform natural gas in a chemical looping process was recently proposed by Jafarian et al. [20]. Their proposed system comprises two inter-connected bubbling column reactors to circulate the liquid hydro-dynamically. Their thermodynamic analysis shows that the extent of conversion of the natural gas to CO_2 and H_2O depends strongly on the molar flow rate of the liquid oxygen carrier (LOC) between the air and fuel reactors. A molar flow rate of LOC between the reactors greater than the stoichiometric value is required for the complete conversion of the fuel to H_2O and CO_2, while a flow rate lower than this results in carbon monoxide production. However, no similar assessment of the potential of other metals or fuels has been performed previously.

The process of gasification of carbon-containing feedstock with different molten metal oxides was recently investigated by Sarafraz et al. [21, 22]. They showed that the production of high-quality syngas with the chemical looping of molten metals such as molten copper, lead and antimony oxides is thermodynamically realistic. They showed that both the ratios of LOC to fuel and that of the gasifying agent to fuel influence the ratio of H_2 to CO in the syngas product. However, the maximum value for H_2: CO achieved with that particular process is 2.05, while its operating temperature of 1350°C is technically challenging to achieve. Furthermore, all of the reactions in that process are exothermic, which makes it difficult to employ solar thermal energy to drive the reaction. Hence, it is desirable to explore the use of other materials to seek to identify any that can offer a higher quality of syngas, a lower operating temperature, and/or the potential to introduce solar energy into an endothermic reaction.

The present investigation aims to assess the thermodynamic potential of a LCLG cycle that employs molten lead as the oxygen carrier, graphite as a surrogate for the carbonaceous

feedstock and steam and/or CO_2 as the gasifying agent. It aims to assess the influence of different operating parameters such as temperature, ratio of LOC/fuel, steam/fuel and CO_2/fuel on the quality of syngas product. It also aims to assess the energetic performance of a system in which the thermal energy from the hot gases is recovered using a supercritical steam power cycle.

2. Conceptual design and modelling

Figure 1 presents a schematic diagram of the key components of a plausible configuration of the LCLG system for the gasification of a solid carbonaceous feedstock. Here we have chosen graphite as a surrogate for more realistic carbon-containing fuels since its properties are well understood. Steam and CO_2 were both considered as alternative or blended gasifying agents with a view to identifying a mechanism to control the ratio of H_2: CO via the main gasification, Boudouard and water gas shift reactions.

The cycle was assessed assuming a plausible configuration of interconnected bubble column reactors for the fuel and air reactors (see Fig. 1), in which a gasifying agent is bubbled through the molten metal oxide, while air is bubbled through the molten metal in the air reactor. Bubble reactors are chosen here because they are known to provide high rates of heat and mass transfer. Impurities in the fuel and gasifying agent are assumed to be separable from the liquid metal, such as by means of a disk-shaped centrifugal ash separator as proposed previously [23]. Molten lead oxide has been selected as the oxygen carrier because the temperature required for its oxidation and reduction reactions lies between 888°C and 1000°C. This range of temperature is within the range of many industrial processes. In addition, the oxidation reaction of molten lead oxide with air is exothermic while the reduction reaction of molten lead oxide with carbon is endothermic. Accordingly, the bubble reduction reactor can also be hybridised with solar

thermal energy to allow the possibility for some of the heat required for the gasification from the solar energy. However, this assessment is beyond the scope of the present work.

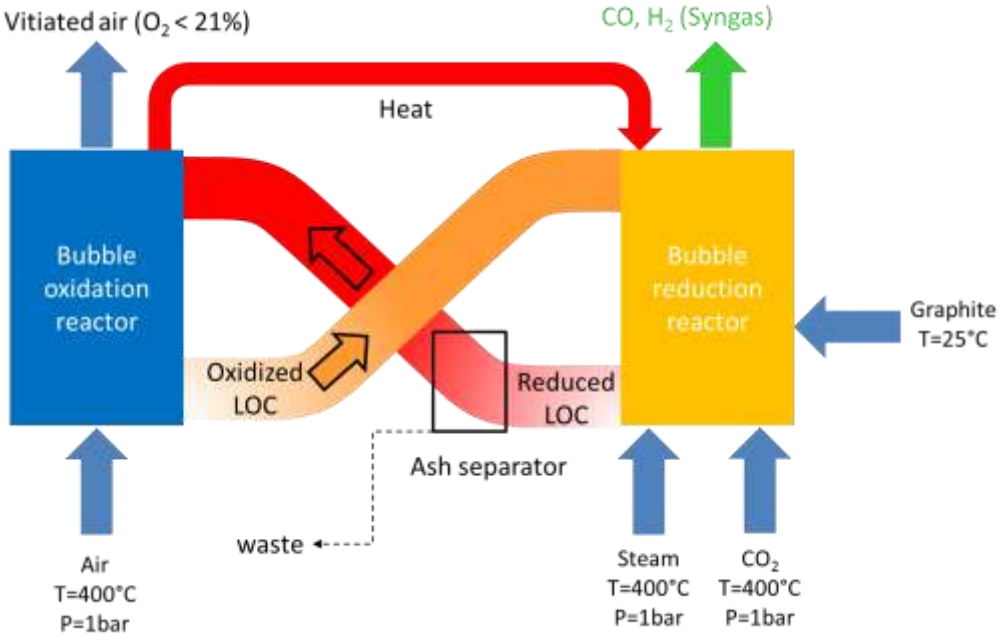

Fig.1. A Schematic diagram of the proposed liquid chemical looping gasification system operated with molten lead oxide.

As can be seen from Fig. 1, the LOC is circulated between the two reactors, which together provide the required heat and oxygen for the gasification reactions. For the present thermodynamic assessment, the following assumptions have been made:

1. The residence time within the reactors is sufficient for the reactions to reach equilibrium so that the Gibbs minimization method can be applied to estimate the equilibrium compositions in the gas and liquid phases.
2. Heat losses from the fuel and air reactors are negligible.
3. A system is available to transfer the LOC between the air and fuel reactors (e.g. fluid-mechanically) with a negligible energy penalty.

4. No solidification occurs in the system, i.e. the conditions are sufficiently far from any solid-liquid two-phase regime.
5. Any impurities in the fuel have a negligible influence on the reactions, so that the only elements involved in the reactions are carbon, hydrogen, oxygen and lead.
6. The sensible heat transferred via the circulation of the LOC, together with the internal transport of heat, is sufficient to satisfy all requirements for heat.
7. Steam and CO_2 enter the fuel reactor at a temperature and a pressure of 400°C and 1 bar, respectively, while the solid fuel is fed into the reactor at 25°C and 1 bar. The outlet temperatures from the fuel and air reactors are the same as those of the corresponding reactor.

For the proposed concept, separate water gas shift reactor is avoided and steam is directly injected into the reactor. The reason for the direct injection of steam to the reactor is:

1) It proceeds the water gas shift reaction and increases the syngas quality with more hydrogen production.
2) It also avoids using a separate water gas shift reactor, which is favourable as it increases the economic viability and reduces the energy required for the start-up.
3) Following the concept of interconnected bubble column reactors, proposed by Jafarian et al. [20], the injection of the steam into the fuel reactor, together with the fuel, can induce further lift within the reactor, which in turn can lead to an efficient circulation of the LOC between the air and the fuel reactors.
4) Injection of steam into the fuel reactor can also lead to the enhancement in mass and heat transfer within the fuel reactor through increasing of mixing.

Figure 2 presents the phase diagram of lead oxide as a function of oxygen mass fraction and for various values of temperature. As can be seen, the region confined by the red rectangle

comprises liquids in the form of PbO and Pb [24]. Therefore, this regime is suitable for operating the LCLG process. In other regions of the phase diagram, lead oxide comprises either a two-phase (solid-liquid) slag or solid-phase material (e.g. T=888 ºC), which are unsuitable for LCLG and do not offer high rates of heat and mass transfer.

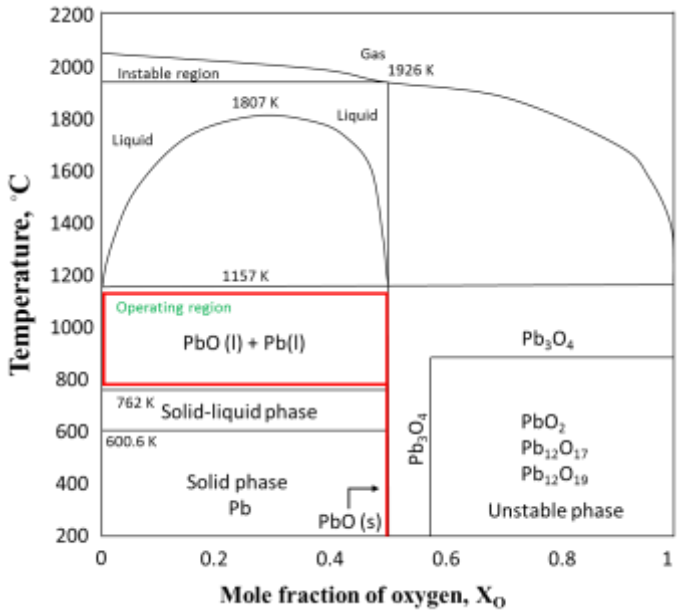

Fig. 2. The dependence of the state of various lead oxide compounds on temperature and mole fraction of oxygen reproduced from previous work [25, 26].

Figure 3 presents the dependence on temperature of the partial pressure of gas-phase oxygen in a molten system of Pb-O-C-N-H. As can be seen, for operating temperatures in the range 888°C < T < 1200°C, PbO (δ) can be in form of stable PbO (l) or Pb (l) or a mixture of PbO (l) and Pb (l). In addition, Table 1 shows the potential reactions in the fuel and air reactors. As can be seen, the reduction reaction for molten lead oxide with carbon has a very large equilibrium constant meaning that the forward reaction proceeds towards completion. Thus, the molten lead oxide from the fuel reactor is predominantly in form of Pb (l). Similarly, the equilibrium constant for the oxidation reaction of Pb (l) with air is also large, so that the molten lead at the outlet of the air reactor is predominantly in form of PbO (l).

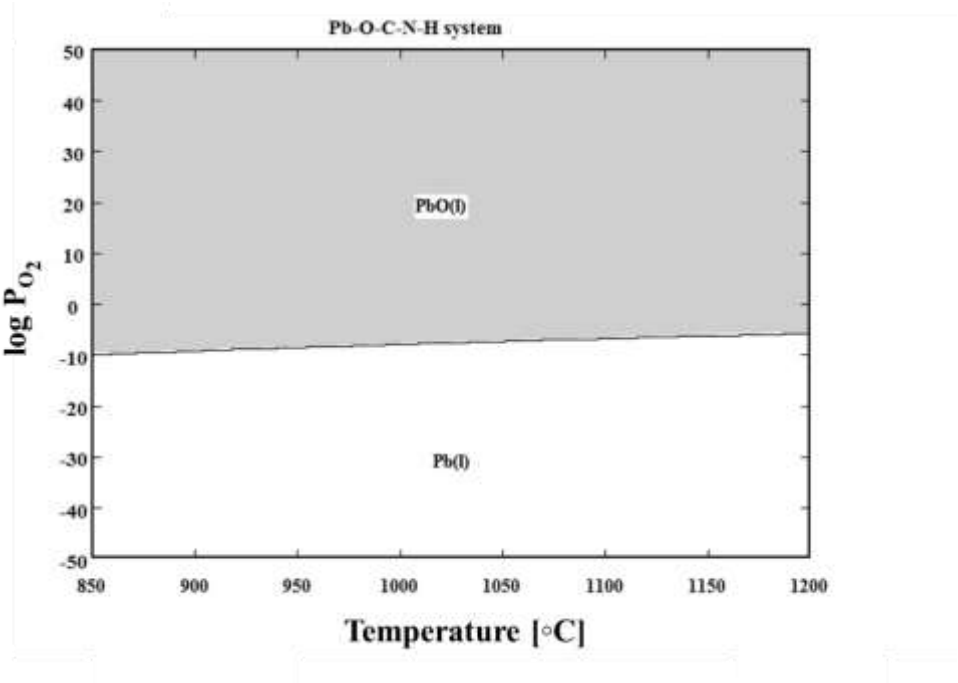

Fig. 3. Phase stability diagram of molten lead and lead oxide showing the dependence on temperature of the oxygen partial pressure.

3. Methodology

The reduction of the oxygen carrier Me_aO_b to Me_cO_d with $C_nH_{2m}O_p$ (as the fuel) within the fuel reactors and its re-oxidation with O_2 from the air in the air reactor is described as follows:

- In the fuel reactor (the general reaction):

$$dC(s) + \frac{2d}{b} Me_aO_b(l) \xrightarrow{Heat} \left[\frac{2ad}{bc}\right] Me_c(l) + dCO_2(g), \quad \text{(R1)}$$

$$dC(s) + \frac{d}{b} Me_aO_b(l) \xrightarrow{Heat} \left[\frac{ad}{bc}\right] Me_c(l) + dCO(g) \quad \text{(R2)}$$

$$CO(g) + H_2O(g) \longrightarrow CO_2(g) + H_2(g) \quad \text{(R3)}$$

- In the air reactor (the general reaction):

$$\left[\frac{a}{c}\right] Me_cO_d(l) + \left[\frac{bc-ad}{2c}\right] O_2(g) \rightarrow Me_aO_b(l), \quad \text{(R4)}$$

The mole fraction of oxygen available in the molten lead (X_o) determines the final composition of the mixture. Since, $n_{PbO\,(\delta)} = n_{PbO\,(l)} + n_{Pb(l)}$. An atom balances with the assumption that $n_{PbO\,(\delta)} = 1$ result in the following equations:

$$n_{Pb} = \frac{2X_o - 1}{X_0}, \tag{1}$$

$$n_{PbO} = \frac{1 - X_o}{X_0}, \tag{2}$$

where,

$$X_o = \frac{n_O}{n_{Pb} + n_O}. \tag{3}$$

Here, X_o is the mole fraction of oxygen in molten lead oxide, while n_o and n_{Pb} are the number of moles of oxygen and Pb in molten lead, respectively. For example, for Xo=0.5, PbO (δ) is in form of PbO (l). In addition, from the reactions presented in Table 2, for the fuel and air reactor, the fraction of PbO (l) and Pb (l) can be obtained for any temperatures and partial pressure of oxygen.

To assess the partial pressure of oxygen in molten lead oxide inside the air reactor, following equation was used:

$$P_{air\,reactor,inlet} = \frac{y_{O_2,equilibrium} \times 101325}{0.21}. \tag{4}$$

Here $y_{O_2,\,equilibrium}$ is the mole fraction of the oxygen in the outlet of the air reactor, which is in equilibrium with the mole fraction of oxygen in molten lead oxide and can be obtained from Fig. 3. So that the inlet air to the air reactor can be obtained.

Table 1. Reactions occurring in the fuel and air reactors.

No.	Reaction	Equilibrium constant (K)			Enthalpy (kJ/mol)		
	Main reactions in the fuel reactor	900ºC	1000ºC	1100ºC	900ºC	1000ºC	1100ºC
R(5)	$PbO(l)+C(s) \Leftrightarrow Pb(l)+CO(g)$	1.05E+5	1.94E+5	3.21E+5	77.028	74.54	72.04
R(6)	$PbO(l)+CO(g) \Leftrightarrow Pb(l)+CO_2(g)$	2.93E+3	1.39E+3	7.29E+2	-91.81	-93.2	-94.56
R(7)	$PbO(l)+H_2(g) \Leftrightarrow Pb(l)+H_2O(g)$	3.81E+3	2.35E+3	1.53E+3	58.67	61	63.26
R(8)	$C(s)+O2(g) \Leftrightarrow CO_2(g)$	4.31E+17	1.79E+16	1.18E+15	-394.9	-395.1	-395.3
R(9)	$CO_2(g)+C(s) \Leftrightarrow 2CO(g)$	3.59E+1	1.39E+2	4.4E+2	168.8	167.7	166.6
R(10)	$C(s)+H_2O(g) \Leftrightarrow H_2(g)+CO(g)$	135.7	135.54	135.31	2.76E+1	8.23E+1	2.1E+2
R(11)	$CO(g)+H_2O(g) \Leftrightarrow H_2(g)+CO_2(g)$	7.68E-1	5.9E-1	4.74E-1	-33.13	-32.196	-31.3
	Main reaction in the air reactor						
R(12)	$Pb(l)+0.5O_2(g) \Leftrightarrow PbO(l)$	1.39E+9	6.6E+8	5.03E+7	-380.17	-376.5	-372.8

The enthalpy and the net Gibbs free energy change of the reaction can be calculated as follows:

$$\Delta M_{red,r} = \sum_{prod} \Delta M_i^f(T) - \sum_{react} \Delta M_i^f(T). \quad (5)$$

In this equation, *M* denotes either the Gibbs free energy or enthalpy of formation of component *i*, while $\Delta M_i^f(T)$ represents either the Gibbs free energy of formation or the change in enthalpy of formation of the component *i* at a given temperature T. Furthermore, the subscripts "red", "prod" and "react" denote "reduction", "products" and "reactants", respectively. As a measure of the thermodynamics potential of the reaction, the Gibbs free energy is the primary criterion chosen to assess the potential of the LOC for the reaction with graphite and air. It is calculated using the data obtained Barin [27]. The mole fraction of the products was estimated using the Gibbs minimization method and thermochemical analysis.

The influence of various operating parameters on the chemical and energetic performance of the LCLG system was assessed with a sensitivity analysis of thermochemical potential following earlier work [28, 29] (using HSC chemistry and an Aspen Plus R-Gibbs reactor). In

previous works, for this purpose, φ is defined as the ratio of inlet moles of molten lead oxide to those of carbon feedstock at the inlet to the fuel reactor:

$$\varphi_{LOC} = \frac{\dot{n}_{LOC}}{\dot{n}_{fuel}}. \quad (6)$$

Here, $\dot{n}$ is the molar flow of the liquid oxygen carrier (LOC) and carbonaceous fuel introduced to the fuel reactor. For the CLG configuration, steam is proposed to be used as the gasifying agent to maximise the hydrogen production and increase the H_2: CO ratio. For this gasifying agent, the flow rate of steam fed to the fuel reactor is:

$$\varphi_{steam} = \frac{\dot{n}_{steam}}{\dot{n}_{fuel}}. \quad (7)$$

Here also, $\dot{n}_{steam}$ and $\dot{n}_{fuel}$ are the molar flow rates of the steam and fuel introduced to the fuel reactor, respectively. Similarly:

$$\varphi_{CO_2} = \frac{\dot{n}_{CO_2}}{\dot{n}_{fuel}}. \quad (8)$$

where $\dot{n}_{CO_2}$ is the molar flow rate of CO_2. In LCLG system, to assess the portion of exergy transported by syngas, the following equation was used:

$$\chi = \frac{\dot{n}_{syngas}.LHV_{syngas}}{\dot{n}_{fuel}.LHV_{fuel}}. \quad (9)$$

where, $\dot{n}_{syngas}$ is the molar flow of the outlet syngas from the fuel reactor and LHV is the lower heating value of the syngas, which depends on the H_2: CO ratio. The exergy of the syngas can be calculated with Eq. (10).

$$Ex_{Chem} = \dot{n}_{syngas}.LHV_{syngas}. \quad (10)$$

The net work from the power block comprising a steam turbine less that consumed by the pumps and other auxiliaries is presented in Eq. (11):

$$W_{net} = \sum_{produced} W - \sum_{consumed} W = \sum W_{ST} - \sum W_{pump}. \quad (11)$$

Here W_{ST} is the total work produced by the steam turbine, W_{pump} is the total work consumed by the pump to produce the required pressure. Both parameters were obtained using an Aspen plus process simulator. The mechanical and thermodynamic efficiencies of the turbine and pump were assumed to be 0.9 and 0.92, respectively following previous work [30]. The first law efficiency of the power block (η) can be defined as the ratio of the work produced from the system to the total input energy, as is given in Eq. (12):

$$\eta = \frac{W_{net}}{\dot{n}_{fuel} . LHV_{fuel}}. \quad (12)$$

To assess the fuel conversion following equation is used:

$$X = \frac{\dot{n}_{fuel,initial} - \dot{n}_{fuel,remaining}}{\dot{n}_{fuel,initial}} \quad (13)$$

Here $\dot{n}_{fuel,initial}$, is the amount of fuel introduced to the gasifier and $\dot{n}_{fuel,remaining}$ is the amount of the unreacted fuel during the gasification. In addition, the carbon conversion depends on both the reaction kinetics and the rates of mass and heat transfer within the reactors, which are characterised by the residence time and depend on the configuration of the reactors. However, an assessment of the role of these parameters is beyond the scope of the present work.

To assess the net enthalpy of reaction of system, an energy balance over the fuel and the air reactors were done considering the enthalpies of inlet air and fuel streams, liquid metal oxide, and outlet streams, which are expressed as:

$$\Delta H_{air\ reactor} = \sum_{outlet} H - \sum_{inlet} H \quad (14)$$

and

$$\Delta H_{Fuel\ reactor} = \sum_{outlet} H - \sum_{inlet} H \quad (15)$$

and

$$Q = \Delta H_{LCLG} = \Delta H_{Air\,reactor} - \Delta H_{Fuel\,reactor} = \sum_{prod.} H - \sum_{react.} H \quad (16)$$

Here

$$\sum_{prod.} H = \sum n_i . \Delta H_i \quad (17)$$

and

$$\sum_{react.} H = \sum n_i . \Delta H_i \quad (18)$$

Here n_i is the mole fraction of each component and ΔH_i is the enthalpy of each component. Prod and react are acronyms for products and reactants, respectively. Depending on the sign of the net enthalpy of the system, Q is the required heat to be supplied to the LCLG (when total energy balance of the system is positive) or released heat from the LCLG (when total energy balance of the system is negative. Table 2 presents the list of both reference operating conditions and the range of their possible values.

Table 2. Operating conditions of the fuel reactor for the molten lead LCLG system.

Parameter	**T(°C), (Fuel and air reactors)**	**Log P_{O_2}**		ϕ_{LOC} (mol/mol)	ϕ_{steam} (mol/mol)	ϕ_{CO2} (mol/mol)
		Air reactor (bar)	Fuel reactor (bar)			
Reference condition	900	-0.301	-0.301	1	1	1
Range (min-max)	800-1000	Variable from -50 to +50		0.05-1.5	0.5-3	0-1.6

4. Results and discussion

4.1. Gibbs free energy and enthalpy of the reactions

Figure 4 presents the dependence on temperature of the enthalpy of reaction and the Gibbs free energy of the gasification and oxidation reactions for graphite in the molten lead medium. As can be seen, the Gibbs free energy is negative for both the reduction and oxidation reactions, meaning that they are spontaneous and feasible. For example, at 800°C, the Gibbs free energy of reduction is -250 kJ, while for oxidation it is approximately -221 kJ. At the same temperature, $\Delta H_{ox} > \Delta H_{red}$ and the reduction reaction is endothermic. It can also be seen that the enthalpy of reduction reaction decreases with an increase in temperature, although not by much. For instance, at 800°C, ΔH_{red} =150.8 kJ, while it is 148 kJ at 1000°C. The oxidation reaction is exothermic, i.e. $\Delta H_{ox} < 0$, and the temperature has only a slight impact on ΔH_{ox} so that ΔH_{ox} increases slightly with an increase in the operating temperature of the air reactor.

Figure 5 presents the estimated dependence on temperature of the mole fraction of products for φ_{LOC}=1, φ_{steam}=2, φ_{CO2}=1. As can be seen, the estimated mole fractions of steam and CO_2 are relatively insensitive to variations in temperature. For example, with an increase in the temperature of the fuel reactor from 900 to 1150°C, the mole fraction of CO_2 in the product decreased by ~2% from ~20% to ~18%, while mole fraction of CO is ~17% and remain constant. This is because the equilibrium constant for reaction 6 is sufficiently small for any CO2 produced to be consumed by reaction R (11). Furthermore, reaction 6 proceeds in the reverse direction. However, the magnitude of equilibrium constant for reactions R (5), R (8) and R (12) is quite large (K>>~10^4) so that these reactions can be expected to proceed to completion resulting in only small changes in the mole fraction of CO_2. The same trend is also seen for CO, which is produced with reaction R (5) and is consumed by reaction R (9) which proceeds in the reverse direction. It can also be seen that the products with the greatest mole

fractions are steam and CO_2, which yield 37% and 24.6% at 900°C and 38.7% and 22.8% at 1150°C. This is because there is excess oxygen at the reference condition, which causes the system to operate in the combustion mode. Nevertheless, the syngas quality is still 1.16 if the excess steam is removed from the products (by condensation), with the resulting mole fractions of CO_2, H_2, CO and CH_4 being 39%, 32.8%, 28.2% and 0.00001%.

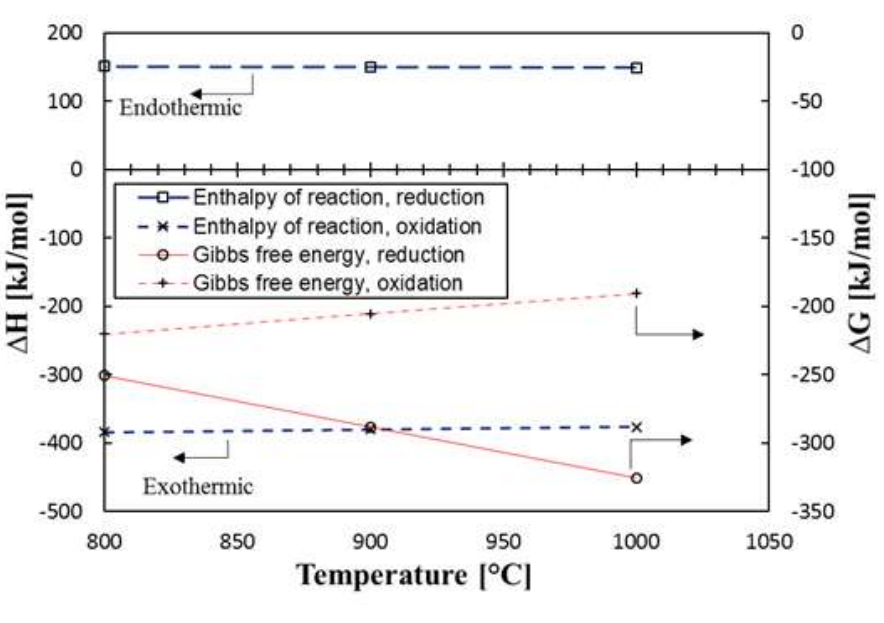

Fig. 4. The calculated dependence on temperature of the enthalpy of reaction and the Gibbs free energy of the reduction and oxidation reactions for molten lead in the fuel and air reactors.

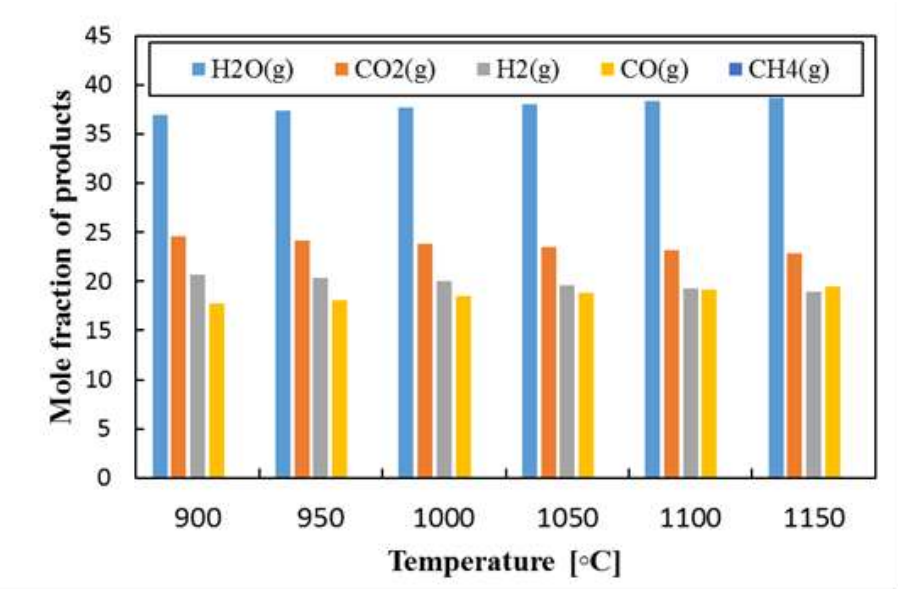

Fig. 5. The calculated dependence on temperature of the mole fraction of products from the fuel reactor for the reference condition given in Table 2.

Figure 6 presents the calculated dependence on temperature of $\frac{\Delta H_{ox}}{\Delta H_{red}}$ for the conditions given in Table 2 for 1 kmol of carbon and steam. As can be seen, $\frac{\Delta H_{ox}}{\Delta H_{red}}$ is highest at 800°C and decreases with an increase in the temperature. However, this change is less than 1%, which means that the net $\frac{\Delta H_{ox}}{\Delta H_{red}}$ is very insensitive to operating temperature. Furthermore, the released heat from the oxidation reactor is 2.5 times larger than that required by the reduction reactor. That is, the process is strongly exothermic, with a net excess energy available for other applications that is insensitive to temperature, making it a relatively stable system and suggesting that there is a little to be gained thermodynamically from operating at temperatures above ~900°C. Note that, some of the released heat in the air reactor is transported with vitiated air, which can be sent to a power block to generate work. Enthalpy of formation of the components is a function of temperature. In figure 6, the enthalpy for the oxidation and reduction reactions based on one mole of fuel has been obtained. Although dependency is not

significant, results show that with an increase in the temperature of the reactors, the ratio of $\Delta H_{ox} / \Delta H_{red}$ decreases. This is because dependency of the enthalpy of formation for reduction reaction is stronger than that of oxidation reaction; thereby an increase in temperature reduces the $\Delta H_{ox} / \Delta H_{red}$ ratio.

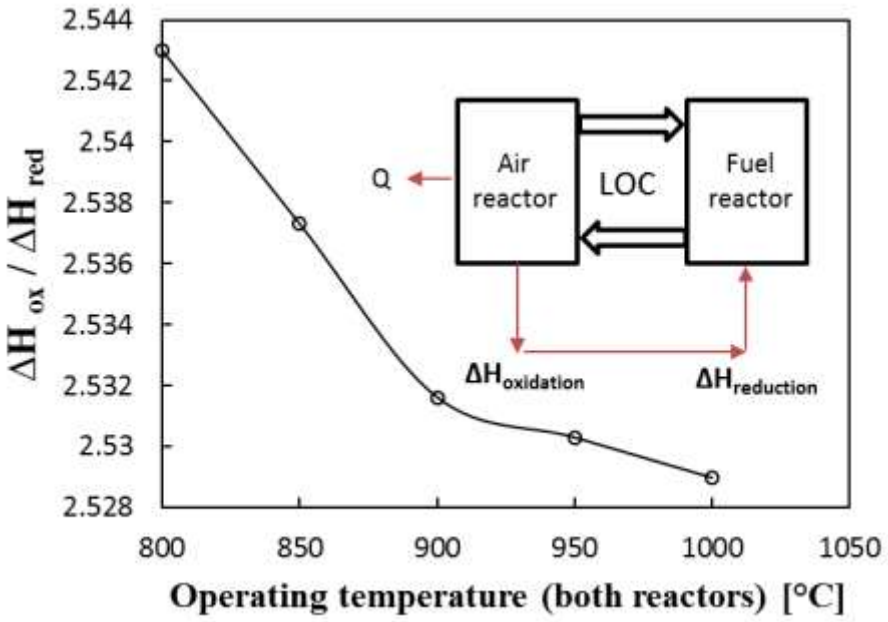

Fig. 6. Calculated dependence on temperature of ratio of enthalpy of reaction of oxidation reactor to that required in the fuel reactor ($\frac{\Delta H_{ox}}{\Delta H_{red}}$). Conditions are as per Table 2.

Figure 7 presents the dependence on temperature of the calculated net enthalpy of the system (Eq.13) on φ_{LOC}. Other operating conditions are as per Table 2. Where $\Delta H_{LCLG} < 0$, the heat released from the air reactor exceeds that required by the fuel reactor. Where $\Delta H_{LCLG} = 0$, they are exactly matched, while where $\Delta H_{LCLG} > 0$, the net process is endothermic. As can be seen, ΔH_{LCLG} decreases with an increase in ϕ_{LOC}, implying that the system becomes more exothermic with an increased role of combustion relative to gasification. Furthermore, the net enthalpy of

the system increases slightly with an increase in the temperature of the reactor, making the system more endothermic. That is, an increase in temperature favours gasification over combustion.

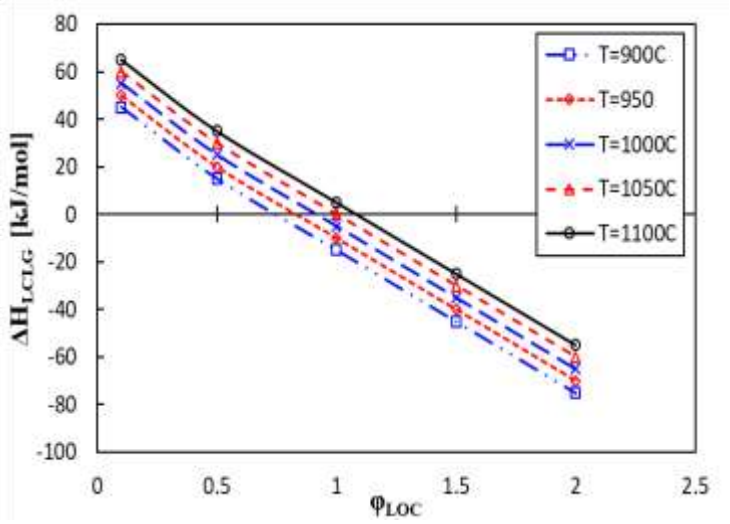

Fig. 7. Calculated dependence of the net enthalpy of the system on the liquid oxygen carrier to fuel ratio for a range of alternative temperatures. Other operating conditions are as per Table 2.

Figure 8 presents the dependence of total enthalpy of the system (Eq.16) on φ_{steam} for a range of alternative temperatures. Other conditions are as per Table 2. As can be seen, the total enthalpy of the system decreases with an increase in φ_{steam}. This is because this increase results in an increase in the proportion of excess steam which results in enthalpy being removed from the system.

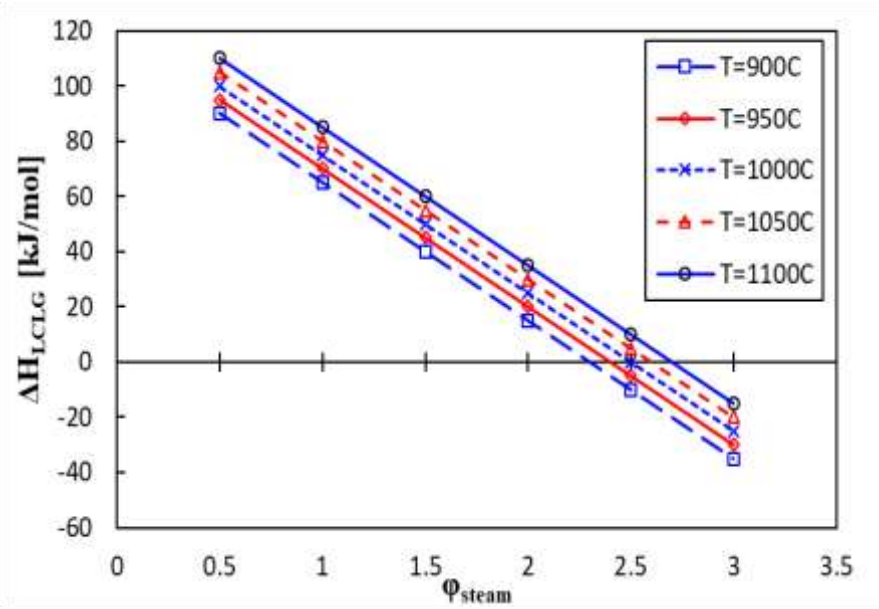

Fig. 8. Calculated dependence of the net enthalpy of the system on the steam/fuel molar ratio for a range of alternative temperatures. Other operating conditions are as per Table 2.

Figure 9 presents the dependence of the total system enthalpy on φ_{CO_2} for a range of constant temperatures. As can be seen, there are two regimes. In one regime, the total enthalpy of the system decreases strongly with an increase in φ_{CO_2} for $0 < \varphi_{CO_2} < 0.05$. This is because, in this range, CO_2 changes the equilibrium such that reaction 11 proceeds in the forward direction resulting in an increase in the enthalpy stored in the syngas (~26% at 900°C). In another regime, for $\varphi_{CO_2} > 0.05$, the decrease is weak. This is because the excess CO_2 removes smaller amount of enthalpy from the reactor (e.g. ~4.9% at 900°C). Overall, at lower values of φ_{LOC} such as $0.01 < \varphi_{LOC} < 0.7$ and $0 < \varphi_{steam} < 3$, the main portion of enthalpy is stored in syngas rather than exhausted gas or vitiated air.

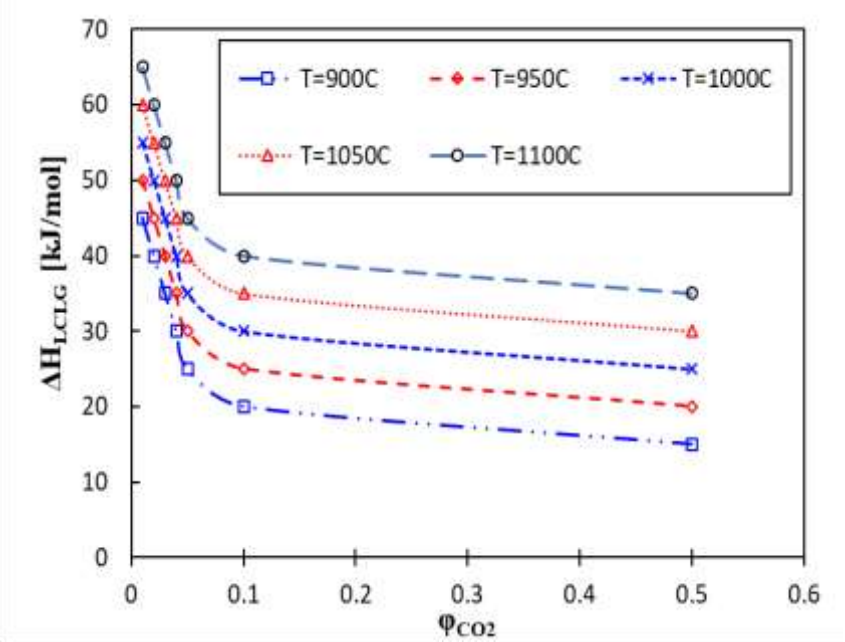

Fig. 9. Calculated dependence of enthalpy of system on CO_2/fuel molar ratio for different temperatures. Other operating conditions are as per Table 2.

4.2. Influence of temperature on mole fraction of gaseous products

Figure 10 presents the calculated dependence on temperature of the mole fraction of the various components of the gaseous products at the reference conditions given in Table 2. It can be seen that the mole fraction of H_2 =0.46 and that of CO = 0.34, which together comprise ~80% of the total mole fraction of gaseous products. Furthermore, the temperature of the gasifier has only a weak influence on the total mole fraction of gaseous products so that the fraction of CO increases by less than 2% over this temperature range. On the other hand, the mole fraction of CO_2 increases with a decrease in temperature. This is because the decrease in the temperature results in the water gas shift reaction to proceed. Although this is undesirable, the total mole fraction of CO_2 is less than 10% and its dependence on temperature is weak so that this disadvantage is small. It should also be noted that these results have been obtained at the reference operating conditions given in Table 2.

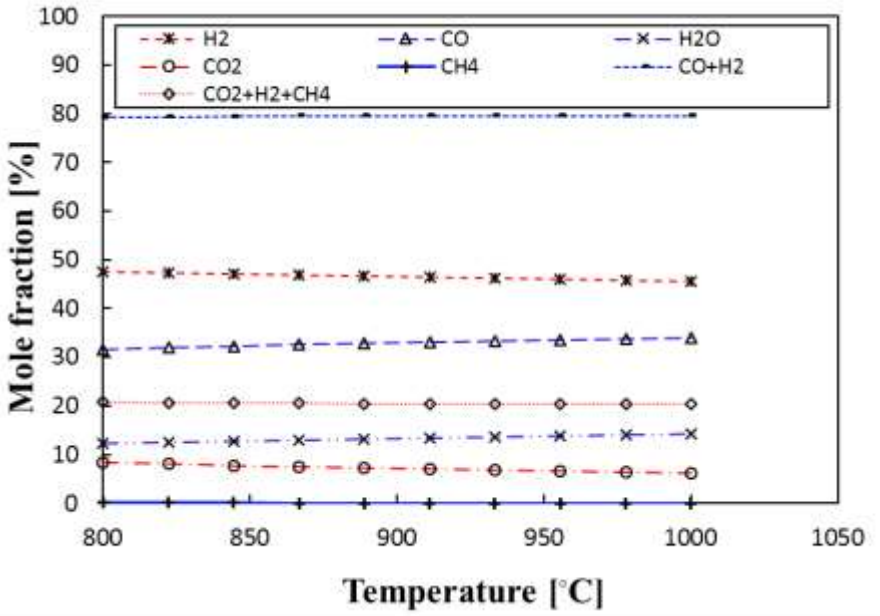

Fig. 10. Calculated dependence of mole fraction of various components of the gaseous product on temperature for the reference conditions given in Table 2.

4.3. Influence of liquid oxygen carrier to fuel on syngas quality

Figure 11 presents the calculated dependence on temperature of the H_2: CO ratio for various values of φ_{LOC}. Other conditions are as per the reference conditions in Table 2. As can be seen, an increase in ϕ_{LOC} leads to a decrease in the quality of syngas. However, this influence is relatively weak at the lower range of temperature. Importantly, an increase in ϕ_{LOC} changes the enthalpy of the system as discussed for Fig. 7. Likewise, operation at the lowest possible temperature also decreases the rate of evaporation of *PbO (l)*, which increases the lifetime of the oxygen carrier and decreases the need for make-up of the LOC.

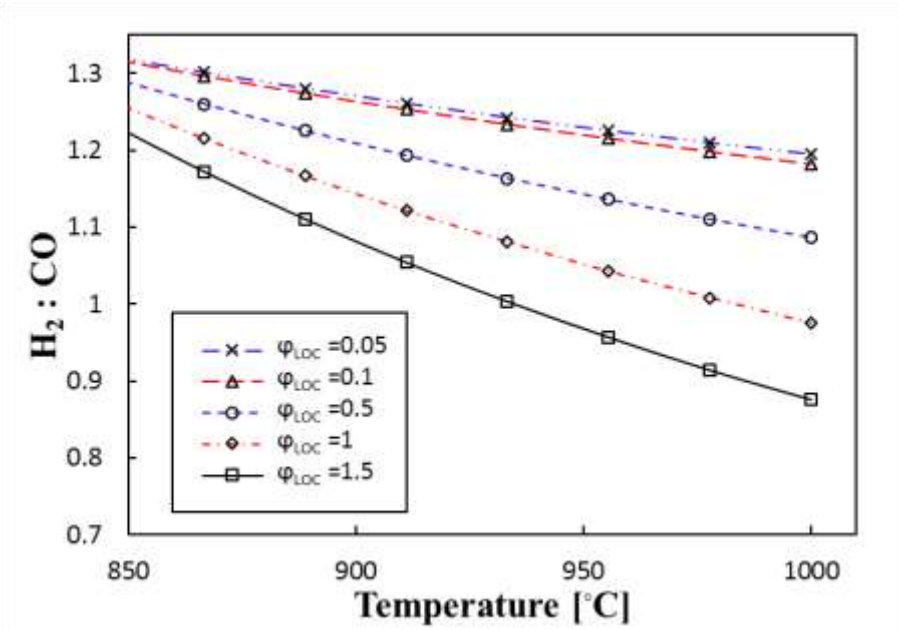

Fig. 11. Calculated dependence on temperature of H_2: CO ratio (syngas quality) for various liquid oxygen carrier to fuel ratios. Other conditions are as per Table 2.

Figure 12 presents the dependence on temperature of the mole fraction of the products for different molar ratios of liquid oxygen carrier to fuel for 100 moles of the carbon. The other operating conditions are as per Table 2. As can be seen, for $\phi_{LOC} = 0.5$, ~43% of the product is H_2 and ~32% is CO, while both the order and the magnitude are different for $\phi_{LOC} = 1.5$ with the dominant component being water, with a mole fraction of ~49%, followed by CO_2 at 30% and both H_2 and CO being ~10%. For higher values of ϕ_{LOC}, the process operates in the combustion mode leading to greater concentrations of H_2O and CO_2.

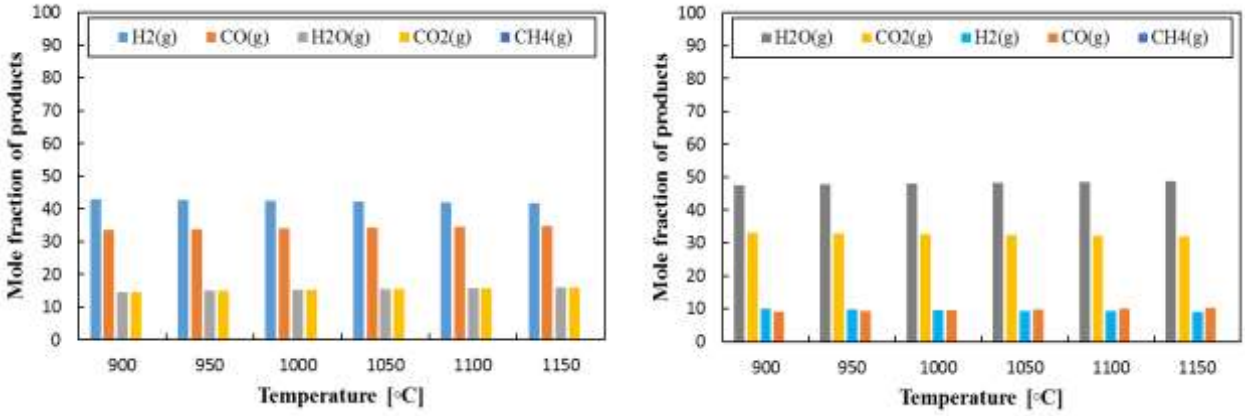

(a) (b)

Fig. 12. Calculated dependence of mole fraction of products on temperature for liquid oxygen carrier to fuel ratios of, a) 0.5 and b) 1.5.

Figure 13 presents the dependence of the moles of products on the ratio of liquid oxygen carrier to fuel at 1000°C for 100 moles of the carbon. The other conditions are as per Table 2. It can be seen that both the mole fractions of H_2 and CO, together with the total mole fraction of the syngas decrease with an increase in φ_{LOC}. However, the total number of moles of exhaust gases (including H_2O and CO_2) increases due to the increase of oxygen in the fuel reactor, which promotes the combustion reactions. For example, for φ_{LOC}=0.01, the number of moles of syngas in the product is ~78, while it is 22 for φ_{LOC}=1.5. In contrast, the total number of moles of exhaust gases increases from ~21 for φ_{LOC}=0.01 to ~78 moles for φ_{LOC}=1.5. Thereby, increase in φ_{LOC} not only decreases the quality of the syngas (H_2: CO) but also reduces the number of moles of the syngas in the products as well.

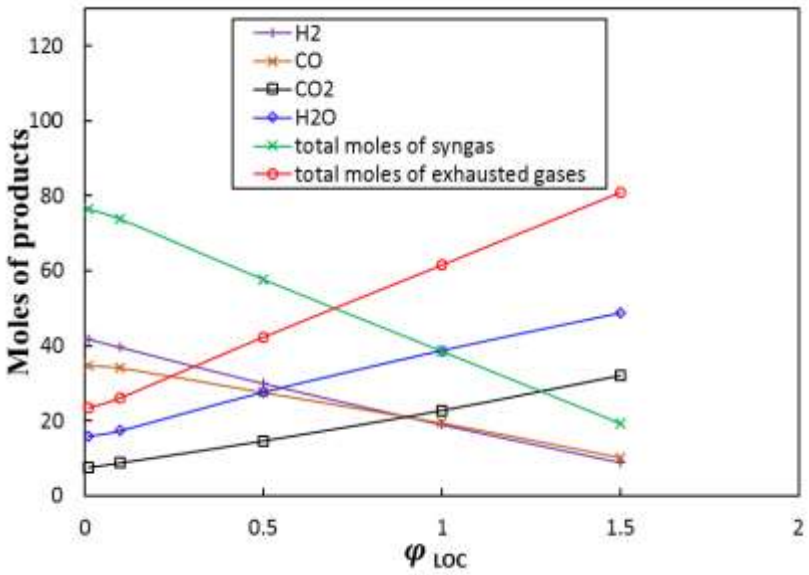

Fig. 13. Calculated dependence of moles of products on liquid oxygen carrier to fuel ratio at 1000°C.

4.4. Influence of the ratio of steam to fuel on syngas quality

Figure 14 presents the dependence on temperature of H_2: CO for various values of φ_{steam}. As can be seen, the quality of syngas is increased both by a decrease in temperature and by an increase in ϕ_{steam}. For example, the syngas quality is increased from 0.76 to 2.3 by an increase in ϕ_{steam} from 0.5 to 3 at a temperature range of 850-1000°C. This further highlights the benefit of operation at the low temperature of the molten regime. Likewise, temperature has a very weak influence on the syngas quality particularly for $0.5 < \varphi_{steam} < 2$, for an increase in temperature from 850°C to 1000°C. However, a significant amount of excess steam is required to achieve the high quality syngas at the expense of mass and enthalpy loss due to the excess steam at the outlet.

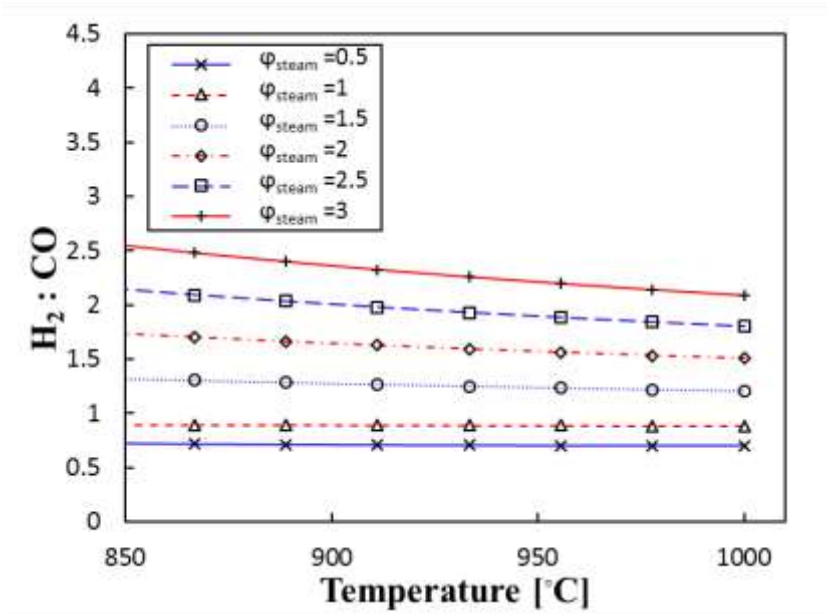

Fig. 14. Calculated dependence on temperature of H_2: CO (syngas quality) for various ratios of steam to fuel. Other conditions are as per Table 2.

Figure 15 presents the dependence on temperature of mole fraction products for different molar ratios of steam to fuel for 100 moles of carbon. Other conditions are as per Table 2 and φ_{LOC} =0.01. As can be seen, more hydrogen is produced with an increase in φ_{steam} up to φ_{steam} =1, beyond which it is decreased slightly. However, excess steam is purged out of the reactor. Therefore, there is a need to employ a condenser to recover the mass and enthalpy loss in form of water and heat, respectively. It is worth saying that portion of enthalpy is also transported and stored in the syngas. As can be seen, for φ_{steam} =0.5, the mole fraction of hydrogen is ~40%, followed by ~58% of CO, while CO_2 and H_2O are both less than 1%. However, for φ_{steam} =3, the mole fraction of hydrogen and CO in the presence of excess steam is 33% and 10%, which can be reach to ~56.1% and ~23.4%, respectively if excess steam is condensed and taken out of the system.

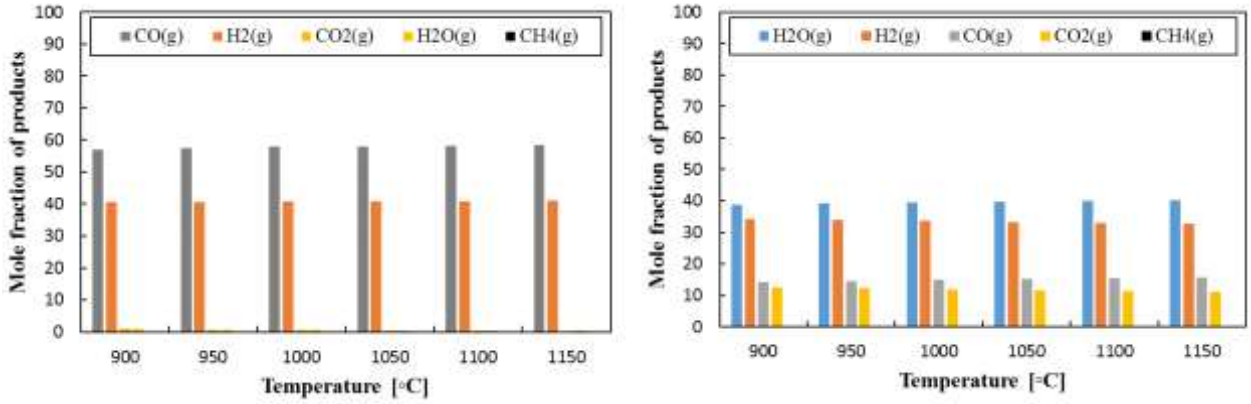

(a) (b)

Fig. 15. Calculated dependence of mole fraction of products on temperature for a ratio of steam to fuel, a) 0.5 b) 3.

Figure 16 presents the dependence of moles of products on steam to fuel ratio at 1000°C. The other conditions are as per Table 2. As can be seen, with an increase in φ_{steam}, the mole fraction of H_2, CO and the total mole fraction of the syngas decreases. However, the total moles of the exhausted gases increase. This is because the presence of steam proceeds the water gas shift reaction and more CO_2 is produced.

Importantly, the quality of syngas (H_2: CO ratio) > 1 at φ_{steam} > 1, while the total moles of the syngas decreases. For example, at φ_{steam} =3, the moles of the syngas is 45 and H_2: CO~2, while total moles of the exhausted gases is 55.

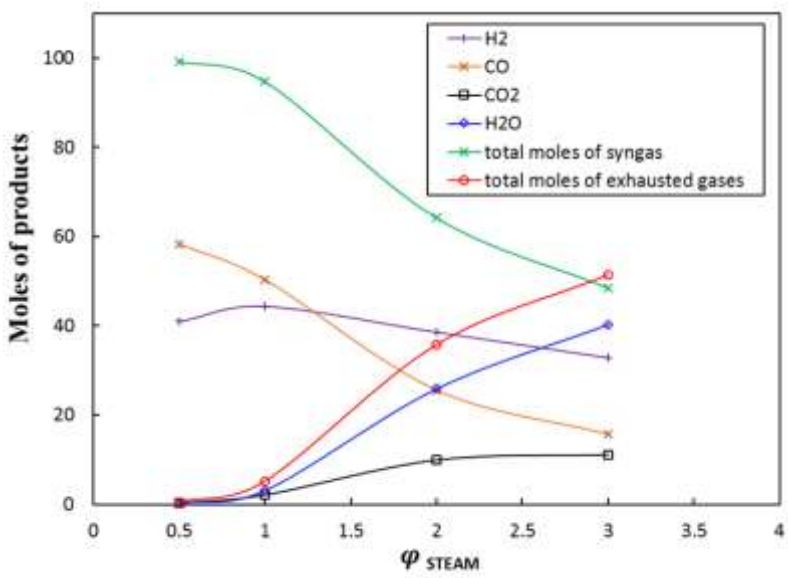

Fig. 16. Calculated dependence of moles of products on steam to fuel ratio at 1000°C.

4.5. Influence of the ratio of CO_2 to fuel on syngas quality

The effect of blending CO_2 with steam as the gasifying agent is presented in figure 17. As can be seen, an increase in the fraction of CO_2 as the gasifying agent decreases the syngas quality. This can be attributed to the role of the equilibrium water-gas shift reaction. Increasing the mole fraction of CO_2 inside the fuel reactor. Overall, the second gasifying agent (here CO_2) offers potential to help to accurately manage the syngas quality, although the influence of CO_2 is generally to lower the syngas quality, which is not desirable for applications such as FTS.

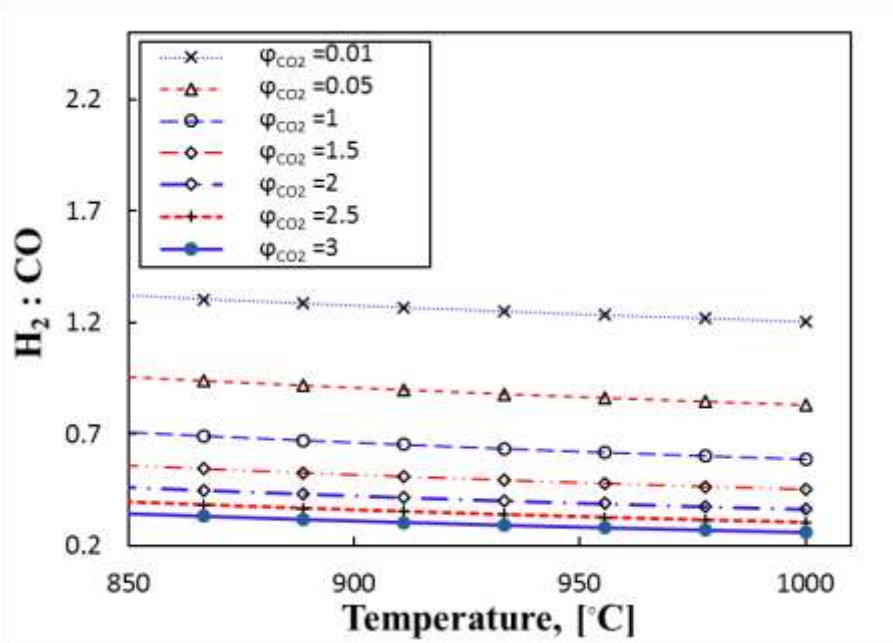

Fig. 17. Calculated dependence of H_2: CO ratio (syngas quality) on the temperature for various ratios of CO_2 to fuel. Other conditions are as per Table 2.

Figure 18 presents the dependence on temperature of mole fraction of products for different molar ratios of CO_2 to fuel. As can be seen, for φ_{CO_2} =1.5, the mole fractions of CO and H_2 are almost the same at ~31 and ~30% respectively. However, for φ_{CO_2} =0.05, the mole fraction of H_2 is insignificantly higher at ~42%, while that of CO is ~32%. The mole fractions of H_2O and CO_2 are significantly lower at ~15% and ~7%, respectively. Furthermore, for φ_{CO_2} > 0.05, the water gas shift reaction is suppressed, which decreases the syngas quality. However, as it was shown from the enthalpy balance, this results in a greater loss of enthalpy through the CO_2 product. Therefore, a value of φ_{CO_2} =0.05, has a good balance of H_2: CO ratio and total product.

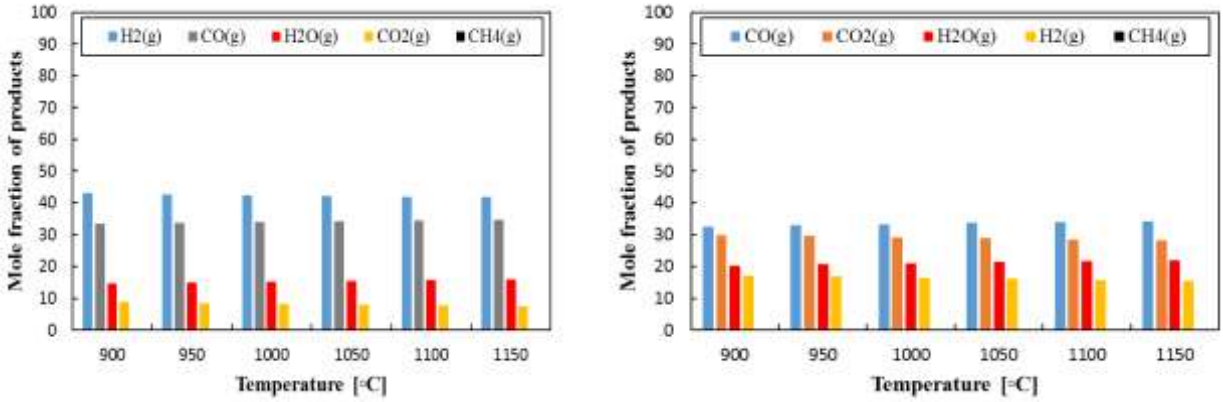

(a) (b)

Fig. 18. Calculated dependence of mole fraction of products on temperature for two different values of CO_2 to fuel ratios, a) CO_2 to fuel ratio =0.05 b) CO_2 to fuel ratio =1.5.

4.6. Influence of the operating parameters on fuel conversion

Figure 19 presents the calculated dependence of fuel conversion on different operating parameters at 1000˚C and 1 bar for the fuel reactor. Here the parameter M can be ϕ_{LOC}, ϕ_{steam} or ϕ_{CO_2}. It can be seen that from these parameters, the proposed LCLG is most sensitive to ϕ_{LOC}. That is, with an increase in ϕ_{LOC}, not only does the fuel conversion increase but the system also changes from the gasification mode to the mixed and complete combustion modes. In the transition regime (mixed combustion-gasification regime), the system simultaneously produces the CO, H_2 and CO_2 in various ratios that depend on the operating conditions. That is, the fraction of CO_2 can be less than, equivalent to or greater than that of CO. It is also notable that the fuel conversion increases linearly with an increase in ϕ_{steam}, albeit with a slope that is lower than that for ϕ_{LOC}. Furthermore, this LCLG process is least sensitive to ϕ_{CO_2}, but displays similar trends to the other parameters.

Overall, three different regimes were identified for the fuel conversion, which are as follows:

- Gasification regime, for which the main products are CO and H_2, while X < 88%,

- Mixed gasification-combustion regime, for which 88% < X < 98% and,
- Combustion for which X > 98%.

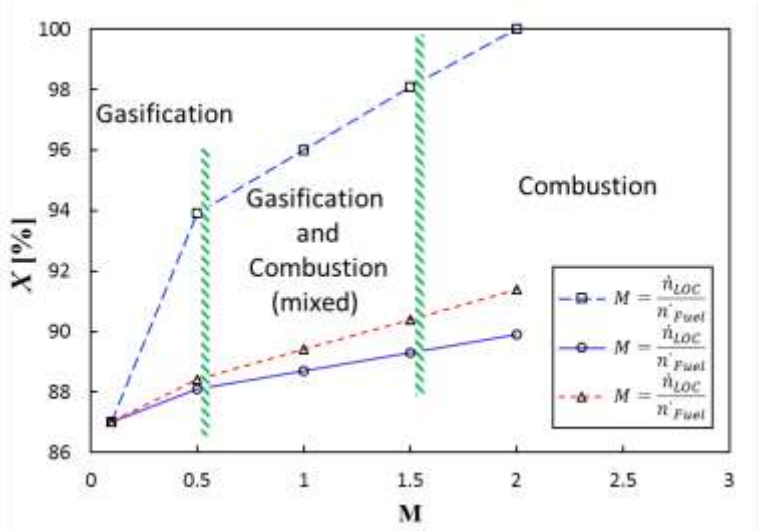

Fig. 19. Calculated dependence of fuel conversion on different operating parameters including liquid oxygen carrier to fuel ratio, steam to fuel ratio and CO_2 to fuel ratio at T=1000°C and P= 1 bar.

4.7. Exergy partitioning

Figure 20 presents the calculated dependence on temperature of net exergy in syngas for various values of ϕ_{LOC}. As can be seen, the net exergy partitioned in the syngas increases with an increase in the temperature, although only slightly. However, it decreases with an increase in ϕ_{LOC}, because the operating mode of the system changes to the chemical looping combustion regime. This decreases the quality of syngas and increases the exergy portioned in the vitiated air. That is, the operating conditions can be chosen to partition the exergy into the syngas or the hot vitiated air preferentially.

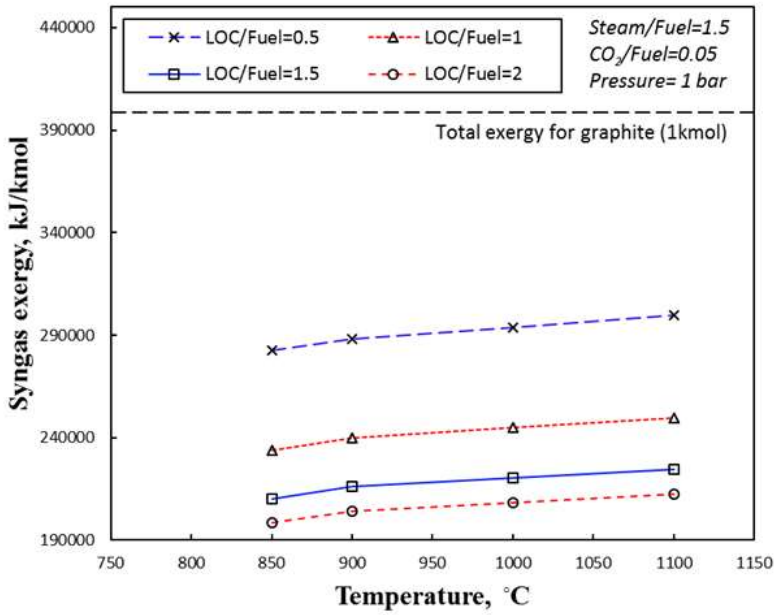

Fig. 20. Calculated dependence on temperature of net exergy of the syngas product for various molar ratios of liquid oxygen carrier to fuel. The molar ratio of steam to fuel ratio is 1.5 and of CO_2 to fuel is 0.05. Other conditions are as per Table 2.

Figure 21 presents the calculated dependence (on a LHV basis) of chemical exergy of the syngas on different operating parameters including ϕ_{LOC}, ϕ_{steam} and ϕ_{CO_2} at 900˚C and 1 bar. As can be seen, the quality of the syngas product and its exergy is maximised (to exceed 287 MJ/kmol) for $0.01 < \phi_{LOC} < 0.7$, $0 < \phi_{steam} < 3$ and $0.01 < \phi_{CO_2} < 0.06$. This regime, however, has the lowest potential to generate work from the hot vitiated air. On the other hand, the production of work with vitiated air is maximised for the regime $\phi_{LOC} > 1$, $\phi_{steam} < 1.7$ and $\phi_{CO_2} > 0.1$.

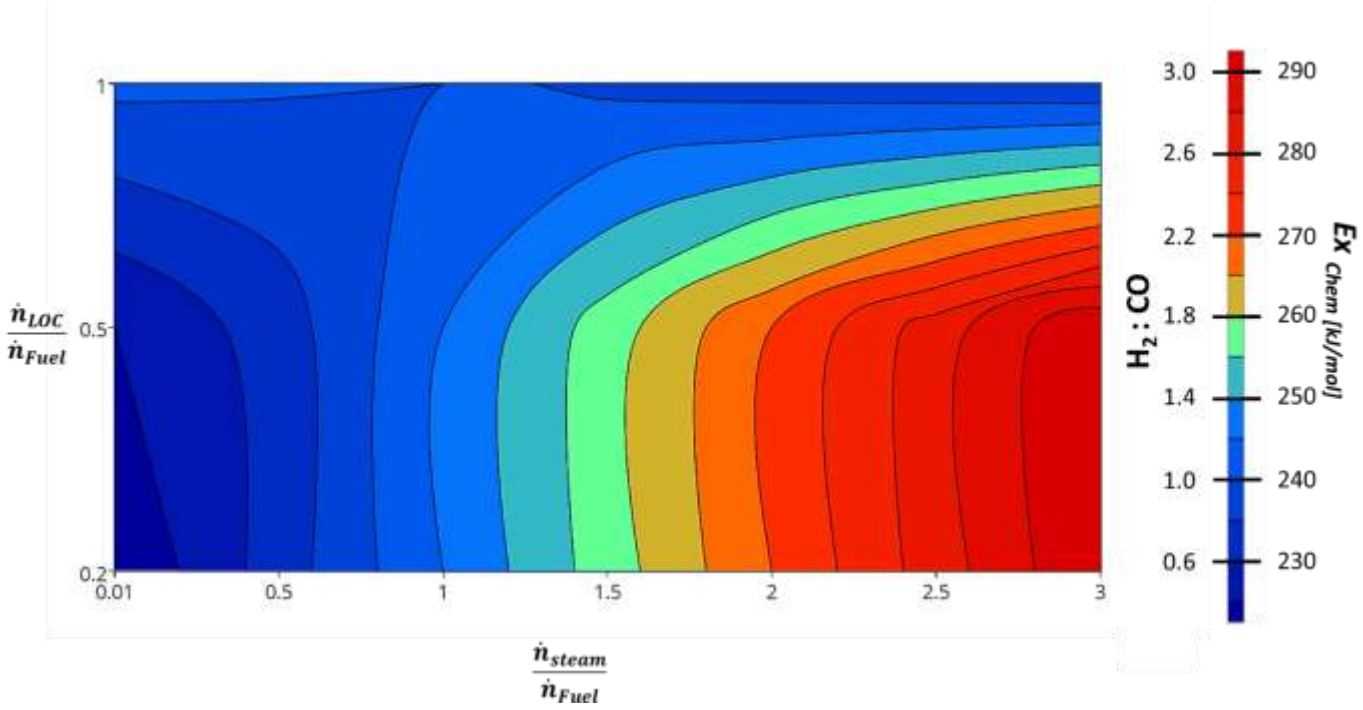

Fig. 21. Calculated dependence of chemical exergy (MJ/kmol) of the syngas product on steam to fuel and liquid oxygen carrier to fuel ratios at T=900°C and at φ_{CO2}=0.05. The other conditions are as per Table 2.

4.8. Power generation plant

Figure 22 presents a schematic diagram of the supercritical steam power plant that was evaluated here to estimate the power generation potential from the outlet streams of the LCLG system. Flow rates, temperatures and pressures of the streams are given in Table 3. Water at 25°C and 1 bar is fed into the pumps to produce high pressure water (streams 3 and 4), which are then fed to two shell and tube heat exchangers. In addition, the outlet streams from the air and fuel reactors (streams 11 and 12) are sent to heat exchangers to recover heat as steam (streams 5 and 6). The steam is then fed to two multi-stage steam turbines to generate work. The outlet from the turbines (Streams 7 and 8) is condensed in two condensers and recirculated. The details of the heat exchanger selected for the process are given in Table 3. The cold outlet stream of the heat exchanger (stream 13) is a cooled syngas, which is fed to a gas to liquid

process or Fischer-Tropsch unit to produce liquid fuels. A three-stage steam turbine was selected for the power block with inlet temperature to turbine of 511-600 ℃ depending on the operating temperature of reactors in LCLG system. The steam turbine inlet temperature was chosen to be 600 ℃, the temperature of stages 1 and 2 and 3 are 428 ℃, 265 ℃ and 143 ℃, respectively and the pressure ratio for each stage is kept constant at 0.255. In addition, the heat loss from the coolers at each stage was 10.4% and the total efficiency of the turbine was 72%.

Table 3. Flow rates and operating conditions of the streams in the proposed supercritical steam power plant.

Parameter*	**1, 10**	**2, 9**	**3*** **	**4*** **	**5**** **	**6**** **	**7**	**8**	**11**	**12**	**13***** **	**14**
T (°C)* [21]	25	25	26.2	25.6	511-600	511-600	100	100	1000	1000	91.2	78.1
P(bar)	1	1	230	230	230	230	1	1	1	1	1	1
Flow rate *(kmol/hr) **[31]**	24590	16374	24590	16374	24590	16374	24590	16374	52158	34541	52158	34541
Enthalpy (MJ/hr)	-7.03	-4.681	-7.02	-4.67	-5.45	-4.67	-5.88	-3.91	-2.13	1.13	-3.7	0.07
Air *(kmol/hr)	0	0	0	0	0	0	0	0	0	34541	0	34541
Water *(kmol/hr)	24590	16374	24590	16374	24590	16374	24590	16374	0	0	0	0
CO *(kmol/hr)	0	0	0	0	0	0	0	0	34424	0	34424	0
H_2 *(kmol/hr)	0	0	0	0	0	0	0	0	17733	0	17733	0

* Temperature, pressure and flow rates are as per the conditions presented in Sarafraz et al.' work [21] and Taimoor et al.'s work [31] respectively. Uniquac was used as the thermodynamic model for liquid phase and for the gas phase modified Peng-Robinson equation of state was employed; **obtained from the HSC chemistry simulations; *** with the consideration of temperature rise and entropy generation in pumps; ****temperature of streams 5 and 6 depends on the operating temperature of the air and fuel reactors; ***** for H_2: CO~0.5.

Table 4. Specifications of the heat exchangers designed* for the power plant.

Total Size (m)	**Type**	**Mount**	**Number (bundle)**	**Surface area per unit, (m^2)**	**Shell number per unit**	**Shell side**	**Tube side**	**Fouling (m^2. K/W)**	**Tube material**	**Shell material**
5.9	BEM	Horizontal	10	105141	40	Air / syngas	Water, (230 bar)	0.005	Carbon steel	Stainless steel

*Designed with HTRI and Aspen Heat Exchanger design.

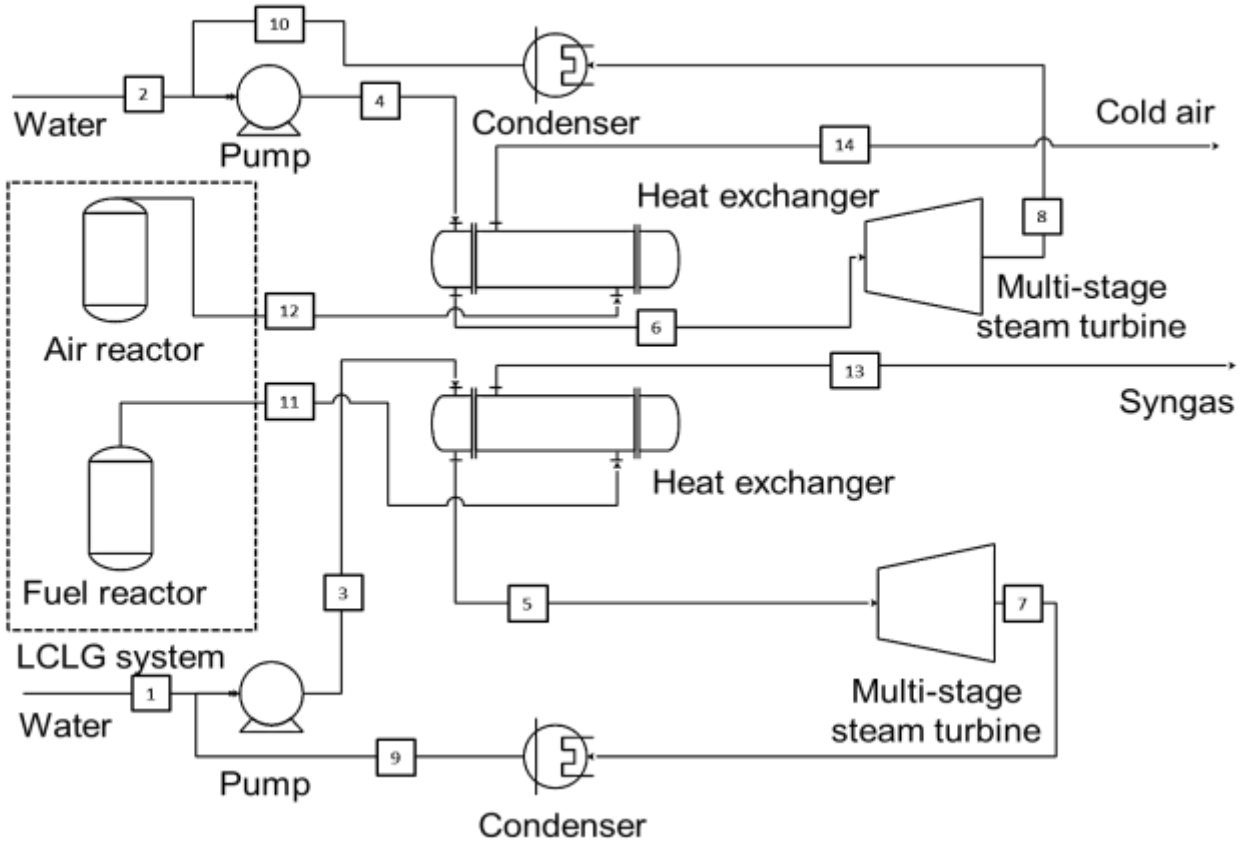

Fig. 22. A schematic diagram of the proposed supercritical steam power plant connected to the outlet streams of the proposed LCLG system.

4.8.1. First law efficiency

Figure 23 presents the calculated dependence of the first law efficiency, Carnot efficiency and the net work on the operating temperature of the reactors. As can be seen, the output from the power plant increases with temperature. This is because the inlet temperature of the steam turbine depends strongly on the operating temperature of the LCLG reactors. At higher operating temperatures of the LCLG system, more thermal energy in form of enthalpy is transferred to power block by exhausted gases. This results in the increase in steam turbine temperature, which causes more work generation in the power block. For instance, when reactors operate at 900°C, the inlet temperature of the steam turbine is 511°C, while when the

temperature of reactors is 1250°C the inlet temperature of turbine is 645°C. Thus, when reactors operate at 900 ˚C, the first law efficiency of power block is 26.1%, which can be increased up to 33.8% at operating temperature of reactors of 1250˚C. However, as discussed in the previous sections, higher temperatures decrease the quality of syngas and mole fraction of gaseous products. Therefore, there is a trade-off between the quality and quantity of produced syngas and the quantity of the produced work in the power plant. Moreover, the work generated with power cycle strongly depends on the circulation of LOC between reactors, which is discussed in section 4.10.2.

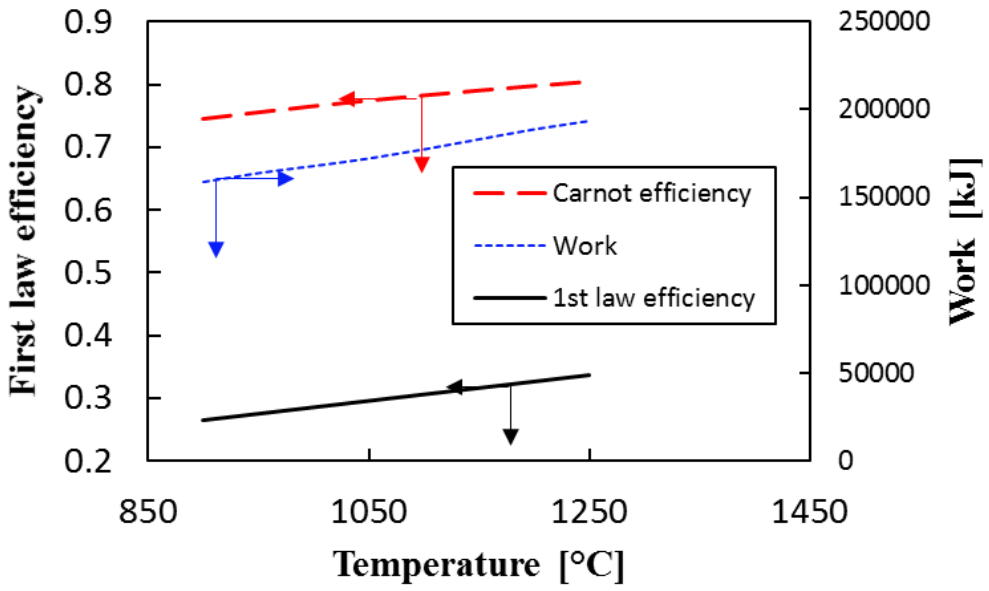

Fig. 23. Calculated dependence of first law efficiency, Carnot efficiency generated work from the power plant on temperature of reactors for φ_{LOC} =1.5.

4.8.2. Exergy partitioning in LCLG

Figure 24 represents the dependence of exergy efficiency of the LCLG system on φ_{LOC}. As can be seen, the exergy of fuel is partitioned between the syngas (As a chemical exergy) and power plant (as the generated work). With an increase in φ the exergy partitioned in the syngas decreases, while exergy transferred to work from the power plant increases. For 0.01 < φ_{LOC} <

0.5, up to ~60% of total exergy is partitioned in syngas. However, for φ_{LOC} > 0.5, exergy partitioned in syngas decreases, while more exergy is transferred to work. For example, for φ_{LOC}=1, the exergy efficiency of the power block can be as high as 56%, while it is 59%, when φ_{LOC}=*1.5*. So, for the case that high-quality syngas is targeted (e.g. H_2: CO=2.05), work generation with power plant decreases. This is because at higher φ_{LOC}, more heat is exchanged between reactors and amount of exergy partitioned in vitiated air increases, however, at lower φ_{LOC}, oxygen is limited in the fuel reactor, which is more favourable for gasification reactions to proceed. Thus, the chemical exergy partitioned in the syngas product increases.

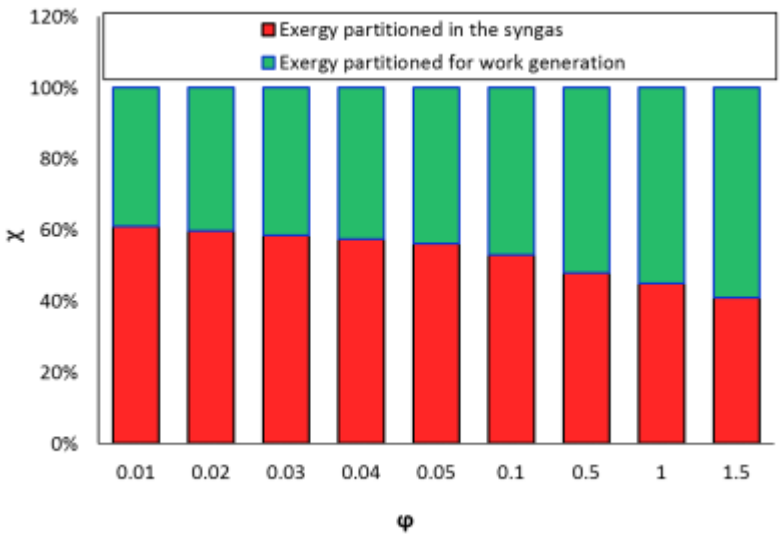

Fig. 24. Dependence of exergy efficiency on molar ratio of LOC to fuel (φ_{LOC}) for the LCLG system excluded the power block.

5. Advantages and technical challenges

The proposed concept working with molten lead offers the potential to bypass some of the key challenges that have plagued chemical looping gasification with solid particles. It also offers the potential for hybridization with concentrated solar energy to drive the endothermic reactions However, the use of molten lead introduces challenges associated with the

solidification and high operating temperature operation. There are also some technical challenges, which need further investigations that come as follows:

1) A High operating temperature: To the best of our knowledge, no continuous flow reactor has been demonstrated for liquid metal oxides at high temperature. For lead oxide, a reactor must sustain temperatures higher than 900°C.

2) Fluid circulation: A method is required to circulate the molten metal at high temperature. To the best of author's knowledge, no such system is commercially available.

3) Heat loss and solidification: For the proposed system, reactors, pipes and other units need to be designed to minimise heat losses and avoid solidification. Furthermore, the temperature difference between operating and freezing points should be sufficiently great, which is difficult to achieve with lead oxide.

4) Robust injection method: It is necessary to avoid local solidification near to the region where the gasifying agent and fuel are injected.

5) Pressure drop across the reactors: The relatively high values of density and viscosity of liquid metal oxides will result in a relatively high pressure drop from circulating fluid in the reactors. Further work will be required to assess the trade-off between pressure drop, which depends on the height of the liquid head, design of the reactor, and parameters such as conversion extent and flow rate. Similarly, the influence of gas holdup will need to be evaluated for the metal oxides.

6) Ash separation: In the present work, the assessment of the proposed system was performed for graphite as a surrogate for any carbonaceous fuel. In case of a fuel with impurity, it is expected that the impurities together with unreacted fuel form an ash layer. Experimental studies of Plevan et al. [32] and Eatwell-Hall et al. [33], demonstrated that ash can be separated from the molten metal due to density difference. Nevertheless, further experimental

investigation is still required and a robust method for the separation of ash from the liquid metal oxides needs to be developed.

6. Conclusions

Significant thermodynamic potential was found for a new concept for the gasification of a solid fuel (assessed here for graphite as a surrogate) using molten lead in a chemical looping gasification with blended gasification agents of steam and/or CO_2. This system showed potential for the gasification of the carbon-containing feedstock and following conclusions were made:

- For the proposed system, the total enthalpy of the system can be positive (endothermic), zero (auto-thermal) and negative (exothermic) depending on φ_{LOC}, φ_{steam} and φ_{CO_2}. Furthermore, the system can be self-sustaining if the rate of circulation of molten lead oxide between reactors is sufficient. For molten lead oxide, the system is self-sustained if φ_{LOC}=0.7 and φ_{steam}=2.5, system is self-sustained.
- The molar ratios of LOC to fuel (φ_{LOC}), steam to fuel (φ_{steam}) and CO_2 to fuel (φ_{CO_2}) in the gasifier can be used to control the quality of syngas from the fuel reactor. Further flexibility is plausible from the blending of CO_2 as a secondary gasifying agent with steam to promote the water gas shift reactions and increase the quality of syngas. For example, for $0.01 < \varphi_{LOC} < 0.7$, $0 < \varphi_{steam} < 3$ and $0.01 < \varphi_{CO_2} < 0.05$, a syngas quality of up to 2.8 can be achieved. However, this also introduces an enthalpy loss due to the excess steam and CO_2. While some enthalpy can be recovered from the steam. However, the recovery process from steam has low efficiency.
- The system offers potential for the power generation by connecting the LCLG system to a supercritical steam power cycle. The maximum first law efficiency and chemical

exergy efficiency of the power cycle was 33.8% and 41%, respectively at 1250°C and for ϕ_{LOC} =1.5.

Acknowledgement:

Authors of this work gratefully acknowledge Australian Research Council (ARC) for the financial support through grant DP150102230. The first author of this work acknowledges "Australian Government Research Training Program Scholarship" for the financial supports.

Nomenclature:

Ex_{chem}	Exergy, MJ/kmol
G	The Gibbs free energy, kJ
H	Enthalpy, kJ/mol
T	Temperature, ˚C
P	Pressure, bar
Q	Heat, kJ
W	Work, kJ
$\dot{n}$	Molar flow rate
X	Fuel conversion
Greek letters	
φ	Operating parameter, see methodology section
Δ	Difference
η	First law efficiency
χ	Exergy efficiency

Subscripts	
ox	Oxidation
red	Reduction
ST	Steam turbine
Abbreviations	
AR	Air Reactor
Eq.	Equation
FR	Fuel reactor
LOC	Liquid oxygen carrier
LHV	Lower heating value, kJ/kmol or kJ/kg
ST	Steam turbine

References

[1] García-Díez E, García-Labiano F, de Diego L, Abad A, Gayán P, Adánez J. Autothermal chemical looping reforming process of different fossil liquid fuels. International Journal of Hydrogen Energy. 2017;42:13633-40.

[2] Ortiz M, Abad A, Luis F, García-Labiano F, Gayán P, Adánez J. Optimization of hydrogen production by chemical-looping auto-thermal reforming working with Ni-based oxygen-carriers. international journal of hydrogen energy. 2011;36:9663-72.

[3] Ortiz M, Luis F, Abad A, García-Labiano F, Gayán P, Adánez J. Hydrogen production by auto-thermal chemical-looping reforming in a pressurized fluidized bed reactor using Ni-based oxygen carriers. International journal of hydrogen energy. 2010;35:151-60.

[4] Pans MA, Abad A, Luis F, García-Labiano F, Gayán P, Adánez J. Optimization of H 2 production with CO 2 capture by steam reforming of methane integrated with a chemical-looping combustion system. International Journal of Hydrogen Energy. 2013;38:11878-92.

[5] Adanez J, Abad A, Garcia-Labiano F, Gayan P, Luis F. Progress in chemical-looping combustion and reforming technologies. Progress in Energy and Combustion Science. 2012;38:215-82.

[6] Kenarsari SD, Yang D, Jiang G, Zhang S, Wang J, Russell AG, et al. Review of recent advances in carbon dioxide separation and capture. Rsc Advances. 2013;3:22739-73.

[7] Qin L, Cheng Z, Guo M, Fan JA, Fan L-S. Morphology evolution and nanostructure of chemical looping transition metal oxide materials upon redox processes. Acta Materialia. 2017;124:568-78.

[8] San Pio M, Roghair I, Gallucci F, van Sint Annaland M. Investigation on the decrease in the reduction rate of oxygen carriers for chemical looping combustion. Powder Technology. 2016;301:429-39.

[9] Liao C, Wu C, Yan Y. The characteristics of inorganic elements in ashes from a 1 MW CFB biomass gasification power generation plant. Fuel processing technology. 2007;88:149-56.

[10] Acharya B, Dutta A, Basu P. Chemical-looping gasification of biomass for hydrogen-enriched gas production with in-process carbon dioxide capture. Energy & Fuels. 2009;23:5077-83.
[11] Li F, Zeng L, Velazquez-Vargas LG, Yoscovits Z, Fan LS. Syngas chemical looping gasification process: Bench-scale studies and reactor simulations. AIChE journal. 2010;56:2186-99.
[12] Fan L-S. Chemical looping systems for fossil energy conversions: John Wiley & Sons; 2011.
[13] Zafar Q, Mattisson T, Gevert B. Integrated hydrogen and power production with CO2 capture using chemical-looping reforming redox reactivity of particles of CuO, Mn2O3, NiO, and Fe2O3 using SiO2 as a support. Industrial & engineering chemistry research. 2005;44:3485-96.
[14] Fan L, Li F, Ramkumar S. Utilization of chemical looping strategy in coal gasification processes. Particuology. 2008;6:131-42.
[15] Tong A, Bayham S, Kathe MV, Zeng L, Luo S, Fan L-S. Iron-based syngas chemical looping process and coal-direct chemical looping process development at Ohio State University. Applied Energy. 2014;113:1836-45.
[16] Anthony EJ. Solid looping cycles: a new technology for coal conversion. Industrial & Engineering Chemistry Research. 2008;47:1747-54.
[17] Chen W-H, Lin M-R, Leu T-S, Du S-W. An evaluation of hydrogen production from the perspective of using blast furnace gas and coke oven gas as feedstocks. international journal of hydrogen energy. 2011;36:11727-37.
[18] Suopajärvi H, Pongrácz E, Fabritius T. The potential of using biomass-based reducing agents in the blast furnace: A review of thermochemical conversion technologies and assessments related to sustainability. Renewable and Sustainable Energy Reviews. 2013;25:511-28.
[19] Bafghi MS, Ito Y, Yamada S, Sano M. Effect of slag composition on the kinetics of the reduction of iron oxide in molten slag by graphite. ISIJ international. 1992;32:1280-6.
[20] Jafarian M, Arjomandi M, Nathan GJ. Thermodynamic potential of high temperature chemical looping combustion with molten iron oxide as the oxygen carrier. Chemical Engineering Research and Design. 2017;120:69-81.
[21] Sarafraz M, Jafarian M, Arjomandi M, Nathan G. Potential use of liquid metal oxides for chemical looping gasification: A thermodynamic assessment. Applied Energy. 2017;195:702-12.
[22] Sarafraz M, Jafarian M, Arjomandi M, Nathan GJ. The relative performance of alternative oxygen carriers for liquid chemical looping combustion and gasification. International Journal of Hydrogen Energy. 2017.
[23] Coats HM. Ash-separator. Google Patents; 1907.
[24] Wriedt H. The O− Pb (Oxygen-Lead) system. Journal of Phase Equilibria. 1988;9:106-27.
[25] Risold D, Nagata J-I, Suzuki R. Thermodynamic description of the Pb-O system. Journal of phase equilibria. 1998;19:213-33.
[26] Jak E, Degterov S, Hayes PC, Pelton AD. Thermodynamic Optimisation of the Systems Cao-Pb-O and Pbo-CaO-SiO2. Canadian metallurgical quarterly. 2013.
[27] Barin I. Thermochemical Data of Pure Substances, Thermochemical Data of Pure Substances: Wiley-VCH; 1997.
[28] Melgar A, Perez JF, Laget H, Horillo A. Thermochemical equilibrium modelling of a gasifying process. Energy conversion and management. 2007;48:59-67.
[29] Li F, Zeng L, Fan L-S. Biomass direct chemical looping process: process simulation. Fuel. 2010;89:3773-84.
[30] Jafarian M, Arjomandi M, Nathan GJ. The energetic performance of a novel hybrid solar thermal & chemical looping combustion plant. Applied Energy. 2014;132:74-85.
[31] Taimoor AA, Muhammad A, Saleem W. Humidified exhaust recirculation for efficient combined cycle gas turbines. Energy. 2016;106:356-66.
[32] Plevan M, Geißler T, Abánades A, Mehravaran K, Rathnam R, Rubbia C, et al. Thermal cracking of methane in a liquid metal bubble column reactor: Experiments and kinetic analysis. International Journal of Hydrogen Energy. 2015;40:8020-33.

[33] Eatwell-Hall R, Sharifi V, Swithenbank J. Hydrogen production from molten metal gasification. international journal of hydrogen energy. 2010;35:13168-78.